MODELING NIGHTGLOW IN ATOMIC OXYGEN RED AND GREEN LINES UNDER MODERATE DISTURBED GEOMAGNETIC CONDITIONS AT MIDLATITUDES

A.V. Tashchilin, L.A. Leonovich

Institute of Solar-Terrestrial Physics SB RAS, Irkutsk, Russia, avt@iszf.irk.ru, lal@iszf.irk.ru

_____

We present results of a study of mid-latitude auroras. The study is based on optical measurements and theoretical modeling. The modeling shows that precipitation can indirectly generate airglow in red and green lines of atomic oxygen by increasing rates of ion formation and heating of thermal electrons. This causes an increase in the rate of dissociative recombination and thermal-electron-collision excitation of the ^1D and ^1S levels.

Keywords Ionospheric disturbance · Upper airglow · Geomagnetic storms · Modeling

_____

INTRODUCTION

An analysis of observational data on atmospheric 557.7 and 630-nm atomic oxygen emissions, which were acquired in Eastern Siberia (52 ° N, 103 ° E) during moderate geomagnetic storms, has revealed disturbances of intensity variations [Leonovich et al., 2012; Leonovich et al., 2015]. Figure 1 illustrates the behavior of parameters of near-Earth space (B_z component of the interplanetary geomagnetic field, solar wind proton density, Dst variations and nocturnal emission intensity of atomic oxygen in the red (630 nm) and green (557.7 nm) lines during weak (April 4–6, 2008: $K_{p\ max}$=5, $A_{p\ max}$=45, Dst=–40) and moderate (September 23–24, 2006: $K_{p\ max}$=7, $A_{p\ max}$=45, Dst=–60; April 5–8, 2010: $K_{p\ max}$=7, $A_{p\ max}$>100, Dst=–80) geomagnetic storms. By comparison, Figure 2 shows variations in the intensity of the emissions for quiet geomagnetic conditions. We can note an increase in the red emission intensity by ≥100 R which is significant for middle latitudes.

To interpret the observed intensity of the atomic oxygen nightglow in the 557.7 nm and 630 lines, model calculations were performed for vertical profiles of volume and integral emissions, which can occur in the nighttime mid-latitude ionosphere under the impact of incoming electron fluxes with different mean and integral energies.

This interpretation is based on the assumption [Leonovich et al., 2015] that electrons penetrate into mid-latitude L shells, where they are trapped, while drifting from the inner magnetosphere under strengthening of the convection electric field during a preceding magnetic storm. Then, during the

next geomagnetic storm, the trapped electrons are intensively scattered by magnetosonic waves [Hasegawa, 1976; Goertz, 1984; Leonovich, Mazur, 1989]. This causes them to precipitate into the lower ionosphere. It is known that trapped charged particles undergo an azimuthal drift, which leads (provide) to their longitudinal distribution up to the daytime sector during strong magnetic storms.

The aim of this work is to study the dependence of the vertical structure of the ionosphere and oxygen emissions on characteristics of precipitating electrons, which can affect the nighttime mid-latitude ionosphere during magnetic storms of varying intensity.

PROBLEM FORMULATION AND METHOD OF INVESTIGATION

Let us consider the mid-latitude upper atmosphere at 90–700 km, which consists of neutral particles (N_2, O_2, O, N, NO), thermal electrons, and ions N_2^+, O_2^+, O^+, N^+, NO^+.
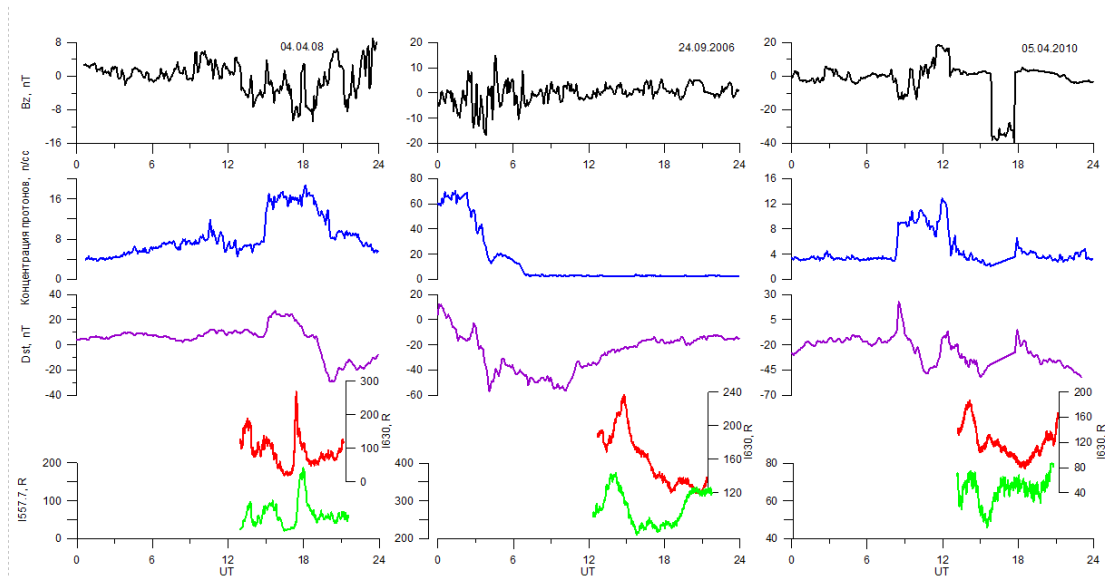

Figure 1. Parameters of near-Earth space and intensities of atomic oxygen emissions in the 557.7 and 630 nm lines during weak and moderate geomagnetic storms
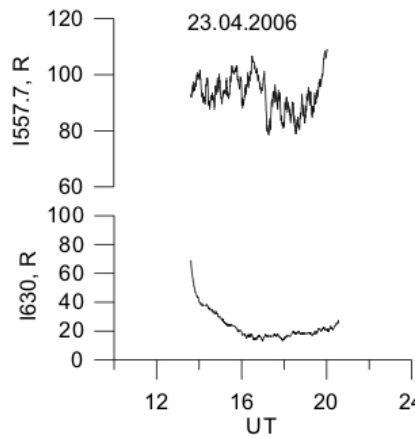

Figure 2. Behavior of the intensity of atomic oxygen emissions in the 557.7 and 630 nm lines under quiet geomagnetic conditions

At night when photoionization is absent, sources of charged particles are the O^+ flux from the plasmasphere P_* through the upper boundary of the ionosphere ($h_* = 700$ km) and the impact ionization of neutral particles by superthermal electrons (STE) precipitating from the inner magnetosphere. We assume that the precipitating electron beam is isotropic in pitch angles and has a Maxwell energy distribution

$$I(E) = \frac{4P_e}{E_{\text{aver}}^3} E \exp\left(-\frac{2E}{E_{\text{aver}}}\right), \text{ cm}^{-2}\text{s}^{-1}\text{eV}^{-1}, \tag{1}$$

where E is the energy, P_e is the integral energy flux in the beam, E_{aver} is the average energy of the beam.

These sources in the ionosphere can ensure stationary height distributions of ionic composition, electron and ion temperatures, energy spectra of STE and oxygen atoms in excited metastable ^1D and ^1S states. The last ones generate oxygen emissions in the red (630 nm) and green (557.7 nm) lines respectively.

Ionic composition

Stationary vertical profiles of O^+ O_2^+, N^+, NO^+ ions are calculated using equations for continuity and motion along geomagnetic field lines in the diffusion approximation [Krinberg, Tashchilin, 1984]:

$$\frac{d}{ds}(n_i V_i) = Q_i + Q_i^{\text{ch}} - \frac{n_i}{\tau_i}, \tag{2}$$

$$-\frac{k}{m_i n_i}\frac{d(n_i T_i)}{ds} - \frac{k}{m_i n_e}\frac{d(n_e T_e)}{ds} + G_{\parallel} = $$
$$= V_i \sum_n \nu_{in} + \sum_j \nu_{ij}^*(V_i - V_j), \tag{3}$$

where s is the distance along the field line related to the height h as $h = s \cdot \sin I$; I is the magnetic field line inclination; $n_e = \sum n_i$ is the electron density; T_e and T_i are electron and ion temperatures; m_i, n_i, V_i are the mass, density, and velocity of i-type ions; Q_i is the rate of ion formation under corpuscular ionization; Q_i^{ch} is the rate of ion formation by chemical reactions; τ_i is the characteristic time of recombination of i-type ions by chemical reactions; k is the Boltzmann constant; ν_{in} and ν_{ij}^* are frequencies of collisions of i-type ions with neutrals and with each other; $G_{\parallel}$ is the projection of the total acceleration of gravity and centrifugal forces on the field line.

The ion density N_2^+ is estimated in the local equilibrium approximation by the formula

$$[N_2^+] = \tau_{N_2^+}(Q_{N_2^+} + Q_{N_2^+}^{\text{ch}}).$$

Chemical reactions between charged and neutral particles, which are included in the model, are listed in the Table.

The rate of ion formation Q_n under impact ionization of n-type neutral particles by energetic (superthermal) electrons is described by [Кринберг, Тащилин, 1984]

$$Q_n(E, h) = 4\pi N_n(h) \int I_n^+(E_p, E)\, \Phi_0(E_p, h)\, dE_p, \tag{4}$$

where $I_n^+(E_p, E)$ is the differential cross-section of ionization of n-type neutral particles by electron impact with resulting formation of a secondary electron with the energy E; $\Phi_0(E_p, h)\, dE_p$ is the isotropic part of the superthermal electron flux with energies from E_p to $E_p + dE_p$ at h.

Ionospheric temperatures

If no distinction is made between temperatures of individual ionic components, equations for heat balance of charged particles in the nighttime ionosphere can be written as [Krinberg, Tashchilin, 1984; Schunk, Nagy, 2009]

$$-\frac{d}{ds}\left(\kappa_e \frac{dT_e}{ds} \right) = Q_e^{\text{CTЭ}} + \sum_i \frac{3m_e}{m_i} n_e \nu_{ei}^* \left(T_i - T_e \right) - \sum_n L_{en}^*, \tag{5}$$

$$-\frac{d}{ds}\left(\kappa_i \frac{dT_i}{ds} \right) = \sum_i 3 n_i \nu_{ie}^* \left(T_e - T_i \right) + \sum_{n,i} \frac{3m_i}{m_n + m_i} n_i \nu_{in} \left(T_n - T_i \right), \tag{6}$$

where κ_e and κ_i are coefficients of electron and ion thermal conductivity along the magnetic field; Q_e^{STE} is the thermal electron heating rate in Coulomb collisions with superthermal electrons; ν_{ei}^*, ν_{ie}^* are frequencies of Coulomb collisions between electrons and ions of different types; L_{en}^* is the electron cooling rate in inelastic collisions with n-type neutrals. As cooling processes we consider the excitation of rotational and vibrational levels of O_2 and N_2 molecules, as well as the excitation of fine-structure transitions of the level ^3P and electronic level ^1D of oxygen atoms. Temperature dependences of L_{en}^* are taken according to [Schunk, Nagy, 2009]. Expressions for collision frequencies and heat conductivity coefficient are taken from [Krinberg, Tashchilin, 1984].

The heating rate of thermal electrons, which is included in heat balance equation (5), is determined by [Krinberg, Tashchilin, 1984]

$$Q_e^{\text{CTЭ}}(h) = 4\pi \kappa n_e(h) \times \left[\Phi_0(E_M, h) + \int_{E_M}^{\infty} \Phi_0(E, h) \frac{dE}{E} \right], \tag{7}$$

where $\kappa = 2.6 \cdot 10^{-12}\, \text{cm}^2 \text{eV}^2$; E_M is the energy at which the general function of distribution of heat and superthermal electrons begins to significantly deviate from the Maxwell one.

Intensity of the red line emission

Emission at 630 nm (red line) occurs during the oxygen atom transition from ^1D to the ground state ^3P. The volume emission (photon·cm^{-3}s^{-1}) of the red line can be calculated from the following relation:

$$\eta_{630} = A_{630}[O(^1D)] = A_{630} \sum_{k=1}^{3} [O(^1D)_k], \tag{8}$$

where $A_{630}=0.00563$ s^{-1} is the Einstein coefficient (the probability of O(^1D) spontaneous emission); [O(^1D)] is the density of excited oxygen atoms in ^1D at a height h, determined from the condition of balance between rates of excitation and deexcitation of the metastable level ^1D. For nighttime mid-latitude conditions we can assume that oxygen atoms in ^1D are formed due to three processes:

- collisions with thermal electrons [Mantas, 1994]:

$$[O(^1D)]_{k=1} = 0.596 \frac{9329+T_e}{(51813+T_e)^3} \times \sqrt{T_e} \exp\left(-\frac{22756}{T_e}\right) \frac{[O]n_e}{L_{630}};$$ (9)

- dissociative recombination of molecular ions O$_2^+$:

$$[O(^1D)]_{k=2} = f(^1D)\alpha_d \frac{[O_2^+]n_e}{L_{630}};$$ (10)

- collisions of oxygen atoms with superthermal electrons:

$$[O(^1D)]_{k=3} = 4\pi \frac{[O]}{L_{630}} \int_{E_{1_D}}^{\infty} I_O^{(^1D)}(E)\Phi_0(E)\,dE.$$ (11)

Here, $f(^1D)=1{,}2$ is the efficiency of formation of excited atoms O(^1D) in the O$_2^+$ dissociative recombination reaction (quantum yield) (its coefficient α_d is given in the table (line 13)); $I_O^{(^1D)}$ is the differential cross-section of ^1D excitation by electron impact; $E_{1_D} = 1.96$ eV is the excitation energy of ^1D; L_{630} is the probability of ^1D deactivation due to spontaneous emission and quenching in collisions with N$_2$, O$_2$, O and electrons, which is determined as [Mantas, 1994]:

$$L_{630} = A_{1_D} + 10^{-11}\left(0.16T_e^{0.91}n_e + 0.8[O] + 2.9\exp\left(\frac{68}{T_n}\right)[O_2] + 2.0\exp\left(\frac{108}{T_n}\right)[N_2]\right), \text{s}^{-1},$$

where $A_{1_D} = 0.00745$ s^{-1}.

The intensity of the integral nightglow in the red line (in Rayleigh) is determined by

$$I_{630} = 10^{-6} A_{630} \int_{h_0}^{h_*} [O(^1D)]\,dh = I_{630}^{\text{th}} + I_{630}^{\text{diss}} + I_{630}^{\text{el}},$$

Reactions considered in the model (T_e, T_i, T_n in K)

	Reactions	Reaction rate coefficients cm^{3}s^{-1}	Source
1	$O^+ + O_2 \rightarrow O_2^+ + O$	$1.6\cdot10^{-11}\left(\dfrac{300}{T_i}\right)^{0.52}, \quad T_i \leq 900\,\text{K}$ $9.0\cdot10^{-12}\left(\dfrac{T_i}{900}\right)^{0.92}, \quad T_i > 900\,\text{K}$	[Hierl et al., 1997]
2	$O^+ + N_2 \rightarrow NO^+ + N$	$1.2\cdot10^{-12}\left(\dfrac{300}{T_i}\right)^{0.45}, \quad T_i \leq 1000\,\text{K}$ $7.0\cdot10^{-13}\left(\dfrac{T_i}{1000}\right)^{2.12}, \quad T_i > 1000\,\text{K}$	[Hierl et al., 1997]

3	$O^+ + NO \rightarrow NO^+ + O$	$7.0 \cdot 10^{-13} \left(\dfrac{300}{T_i} \right)^{-0.87}$	[Richards, 2011]
4	$N_2^+ + O \rightarrow O^+ + N_2$	$7.0 \cdot 10^{-12} \left(\dfrac{300}{T_i} \right)^{0.23}$	[Richards, 2011]
5	$N_2^+ + O \rightarrow NO^+ + N$	$1.33 \cdot 10^{-10} \left(\dfrac{300}{T_i} \right)^{0.44}, \quad T_i \leq 1500\,K$ $6.55 \cdot 10^{-11} \left(\dfrac{T_i}{1500} \right)^{0.2}, \quad T_i > 1500\,K$	[Fox, Sung, 2001]
6	$N_2^+ + O_2 \rightarrow O_2^+ + N_2$	$5.10 \cdot 10^{-11} \left(300 / T_i \right)^{1.16}, \quad T_i \leq 1000\,K$ $1.26 \cdot 10^{-11} \left(T_i / 1000 \right)^{0.67}, \quad 1000 < T_i < 2000\,K$ $2.39 \cdot 10^{-11}, \qquad\qquad T_i > 2000\,K$	[Fox, Sung, 2001]
7	$N_2^+ + NO \rightarrow NO^+ + N_2$	$3.6 \cdot 10^{-10}$	[Richards, 2011]
8	$N_2^+ + N \rightarrow N^+ + N_2$	$1.0 \cdot 10^{-11}$	[Fox, Sung, 2001]
9	$N_2^+ + e \rightarrow N + N$	$2.2 \cdot 10^{-7} \left(\dfrac{300}{T_e} \right)^{0.39}$	[Richards, 2011]
10	$O_2^+ + N_2 \rightarrow NO^+ + NO$	$1.0 \cdot 10^{-15}$	[Fox, Sung, 2001]
11	$O_2^+ + N \rightarrow NO^+ + O$	$1.0 \cdot 10^{-10}$	[Richards, 2011]
12	$O_2^+ + NO \rightarrow NO^+ + O_2$	$4.5 \cdot 10^{-10}$	[Richards, 2011]
13	$O_2^+ + e \rightarrow O + O$	$1.95 \cdot 10^{-7} \left(\dfrac{300}{T_e} \right)^{0.70}, \quad T_e \leq 1200\,K$ $7.39 \cdot 10^{-8} \left(\dfrac{1200}{T_e} \right)^{0.56}, \quad T_e > 1200\,K$	[Richards, 2011]
14	$NO^+ + e \rightarrow N + O$	$4.2 \cdot 10^{-7} \left(\dfrac{300}{T_e} \right)^{0.85}$	[Richards, 2011]
15	$N^+ + O \rightarrow O^+ + N$	$2.2 \cdot 10^{-12}$	[Richards, 2011]
16	$N^+ + O_2 \rightarrow O^+ + NO$	$2.75 \cdot 10^{-11} \left(\dfrac{300}{T_i} \right)^{-0.45}, \quad T_i \leq 1000\,K$ $4.75 \cdot 10^{-11}, \qquad\qquad T_i > 1000\,K$	[Richards, 2011]
17	$N^+ + O_2 \rightarrow O_2^+ + N$	$1.925 \cdot 10^{-10} \left(\dfrac{300}{T_i} \right)^{-0.45}, \quad T_i \leq 1000\,K$ $3.325 \cdot 10^{-10}, \qquad\qquad T_i > 1000\,K$	[Richards, 2011]
18	$N^+ + O_2 \rightarrow NO^+ + O$	$2.425 \cdot 10^{-10} \left(\dfrac{300}{T_i} \right)^{-0.45}, \quad T_i \leq 1000\,K$ $4.275 \cdot 10^{-10}, \qquad\qquad T_i > 1000\,K$	[Richards, 2011]
19	$N^+ + NO \rightarrow N_2^+ + O$	$8.33 \cdot 10^{-11} \left(\dfrac{300}{T_i} \right)^{0.24}$	[Richards, 2011]
20	$N^+ + NO \rightarrow NO^+ + N$	$4.72 \cdot 10^{-10} \left(\dfrac{300}{T_i} \right)^{0.24}$	[Richards, 2011]

where I_{630}^{th}, I_{630}^{diss}, I_{630}^{el} are integral intensities defined by thermal electrons, dissociative recombination of O_2^+ and STE respectively.

Intensity of the green line emission

Emission at 557.7 nm (green line) occurs during the oxygen atom transition from the state ^1S to the metastable state ^1D. The volume emission (photon·cm^{-3} s^{-1}) of the green line can be calculated as follows

$$\eta_{557.7} = A_{557}[O(^1S)] = A_{557}\sum_{k=1}^{3}[O(^1S)_k], \tag{12}$$

where A_{557}=1.18 s^{-1} is the Einstein coefficient (the probability of spontaneous emission of $O(^1S)$); $[O(^1S)]$ is the density of excited oxygen atoms in the ^1S state. For nighttime mid-latitude conditions we assume that oxygen atoms ($O(^1S)$) are formed due to the following processes:

- triple collisions triple collisions of the ground-state $O(^3P)$ atoms [de Meneses et al., 2008]:

$$[O(^1S)]_{k=1} = \frac{4.7\cdot 10^{-33}\left(300/T_n\right)^2[O]^3\left([O_2]+[N_2]\right)}{(A_{1s} + 4.0\cdot 10^{-12}\exp(-865/T_n)[O_2])\left(15[O_2]+211[N_2]\right)}; \tag{13}$$

- dissociative recombination of molecular ions O_2^+:

$$[O(^1S)]_{k=2} = f(^1S)\alpha_d\frac{[O_2^+]n_e}{L_{557.7}}; \tag{14}$$

- collisions of oxygen atoms with superthermal electrons:

$$[O(^1S)]_{k=3} = 4\pi\frac{[O]}{L_{557.7}}\int_{E_{1S}}^{\infty}I_O^{(^1S)}(E)\Phi_0(E)dE. \tag{15}$$

Here, $f(^1S)$=0.02 is the quantum yield of excited atoms $O(^1S)$ in the O_2^+ dissociative recombination reaction; $I_O^{(^1S)}$ is the differential cross-section of ^1S excitation by electron impact; E_{1S}=4.17 eV is the excitation energy of ^1S; $L_{557.7}$ is the probability of ^1S deexcitation due to spontaneous emission and quenching in collisions with O_2, O [de Meneses et al., 2008]

$$L_{557.7} = A_{1S} + 10^{-12}\times\left(0.02[O] + 4.9\exp\left(-\frac{885}{T_n}\right)[O_2]\right), s^{-1},$$

where A_{1S}=1.35 s^{-1}.

The intensity of the integral nightglow in the green line (in Rayleigh) is determined from

$$I_{557.7} = 10^{-6}A_{557}\int_{h_0}^{h_*}[O(^1S)]dh = I_{557.7}^{3O} + I_{557.7}^{diss} + I_{557.7}^{el},$$

where $I_{557.7}^{3O}$, $I_{557.7}^{diss}$, $I_{557.7}^{el}$ are integral intensities caused by triple collisions, dissociative recombination of O_2^+ and STE respectively.

STE energy spectra

It follows from expressions (4), (7), (11), (15) that to calculate the rate of corpuscular ionization and heating, as well as densities of oxygen atoms in the metastable ^1D and ^1S states, we need to know the isotropic part of the superthermal electron flux.

$$\Phi_0(E, h) = \frac{1}{2}\int_{-1}^{1} \Phi(E, \mu, h)d\mu,$$

where $\mu = \cos\vartheta$, ϑ is the electron pitch angle. $\Phi_0(E, h)$ can be calculated using an approximate method [Krinberg, 1978] which represents the pitch angular dependence of STE flux $\Phi(E, \mu, h)$ as a series of Legendre polynomials. If we limit ourselves to two terms of the series (the diffusion approximation) and take

$$\Phi(E, \mu, h) = \Phi_0(E, h) + \mu\,\Phi_1(E, h), \tag{16}$$

then the accuracy of the calculation in the precipitation region $\Phi_0(E, h)$ appears to be sufficient to determine the above integral characteristics describing effects of precipitating STE. Since during inelastic collisions caused by impact ionization and excitation of neutral atoms and molecules the incident superthermal electron deviates little from its travel direction (forward scattering), and the secondary electron is emitted mainly in a perpendicular direction, in order to calculate coefficients in expansion (16) we can obtain the following system of equations [Krinberg, 1978]:

$$\frac{1}{3}\frac{\partial\Phi_1}{\partial s} = \frac{\partial}{\partial E}(M\,\Phi_0) - A\Phi_0 + \frac{1}{4\pi}(Q_s + G_0), \tag{17}$$

$$\frac{\partial\Phi_0}{\partial s} = \frac{\partial}{\partial E}(M\,\Phi_1) - B\Phi_1 + \frac{1}{4\pi}G_1, \tag{18}$$

where $M(E, h) = s_e n_e$; $A = \sum_n \sigma_n^{(*)})N_n$; $B = \sigma_e n_e + \sum_n (\sigma_n^{(*)} + \sigma_n^{(1)})N_n$; $\sigma_n^{(1)}, \sigma_n^{(*)}$ are cross-sections of STE scattered by n-type neutral particles in elastic and inelastic collisions respectively; $s_e = E\sigma_e$; $\sigma_e = \kappa / E^2$; $\kappa = 2.6 \cdot 10^{-12}\,\text{см}^2\text{эВ}^2$. The values of Q_s and G_k on the right side of (17) describe respectively the secondary electron production rate and the electron production rate in the energy range from E to $E+dE$ due to precipitating superthermal electron energy losses in inelastic processes of impact ionization and excitation of neutral particles. They have the following form [Krinberg, 1978]:

$$Q_s(E) = 4\pi\sum_n N_n \sum_\gamma \int_{En\gamma+2E}^{\infty} I_{n\gamma}^+(E', E)\Phi_0(E')dE', \tag{19}$$

$$G_k(E) = 4\pi\sum_n N_n \left[\sum_\gamma \int_0^E I_{n\gamma}^+(\varepsilon, E')\,\Phi_k(\varepsilon)dE' + \sum_\alpha \sigma_{n\alpha}(E + E_{n\alpha})\Phi_k(E + E_{n\alpha})\right], \tag{20}$$

where $\varepsilon = E + E_{n\gamma} + E'$; $I_{n\gamma}^+(E', E)$ is the partial cross-section of ionization of n-type neutral particles by an incident electron with energy E' with resulting production of a secondary electron with energy E and n-type ion in the energy state $E_{n\gamma}$; $\sigma_{n\alpha}(E)$ is the partial cross-section of n-type neutral particle excitation from the ground state to the $E_{n\alpha}$ state by an incident electron with energy E.

101

Energy dependences of scattering cross-sections for elastic collisions $\sigma_n^{(1)}(E)$ were taken from [Rees, 1989]. Differential and total cross-sections of ionization, excitation, and inelastic scattering of electrons in collisions with neutrals $I_{n\gamma}^+(E', E)$, $\sigma_{n\alpha}(E)$, $\sigma_n^{(1)}(E)$ are calculated using the analytical expressions presented in [Banks et al., 1974].

The system of equations (2), (3), (5), (6), (17), and (18) is solved numerically with the methods described in [Krinberg, Tashchilin, 1984]. Boundary conditions are specified as follows.

At the lower boundary (h_0=90 km), ion densities are defined in the local equilibrium approximation as the solution of algebraic equations

$$n_i = \tau_i (Q_i + Q_i^{\text{ch}}).$$

Electron and ion temperatures are found from the heat equilibrium condition $T_e = T_i, = T_n$, and the superthermal electron flux is assumed to be isotropic, i.e. $\Phi_1(E, h_0) = 0$.

At the upper boundary (h_*=700 km), we preset an oxygen ion flux incoming from the plasmasphere such that $P_*=10^8$ cm^{-2} s^{-1}. Fluxes of other ions are set equal to zero. Electron and ion heat balance equations are solved under the condition of absence of heat fluxes at the upper boundary. STE transport equations (17), (18) are solved in the energy range from 1 eV to $E_{\max}=10^4$ eV with the energy boundary condition $\Phi_0(E_{\max}, h)=\Phi_1(E_{\max}, h)=0$. At the upper boundary h_*, we prescribe the isotropic spectrum of precipitating electrons of the form of (1).

MODEL RESULTS

The response of the nighttime mid-latitude ionosphere to energetic electron precipitation events is modeled for the geographic point with coordinates 52° N and 105° E under moderately disturbed geomagnetic conditions (K_p=4, A_p=30) and moderate solar activity (F10.7=110) in the equinoctial season. To describe spatio-temporal variations of temperature and densities of neutral components O, O$_2$, N$_2$, N, and NO, we employ the global empirical model of the thermosphere NRLMSISE-00[Picone et al., 2002] Parameters of the ionosphere and oxygen emissions are computed for the following characteristics of beams of incoming superthermal electrons:

- the integrated energy flux P_e=0.1÷3.5 with a step of 0.1 (erg·cm^{-2}·s^{-1});
- the average beam energy E_{aver}=0.1, 0.5, 1.0, 2.0, 4.0 (keV).

Figure 3 shows estimated distributions of the electron density n_e, electron temperature T_e, volume emissions in the red O(^1D) and green O(^1S) lines in coordinates h–P_e with different average energies of precipitating electrons.

Let us consider the properties of the ionosphere and oxygen emissions obtained from the modeling, which are formed under the action of only two factors – the inflow of thermal ions from the overlying plasmasphere and superthermal electron precipitation.

Figure 3 indicates that the dependence of the ionosphere structure and airglows on the energy of precipitating electrons at $E_{aver} \leq 1$ keV ("soft" precipitation) greatly differs from the similar dependence at $E_{aver} \geq 1$ keV ("hard" precipitation). In the first case, $n_e(h)$ profiles have one peak with quite high values $n_{e\,max} \sim 10^6$ cm^{-3}, which are proportional to P_e and localized above 200 km, i.e. substantially below the height of the nighttime maximum of the normal F2 layer. This is explained by the fact that low-energy precipitating electrons begin to lose their energy at fairly great heights ($h \geq 300$ km) due to large cross-sections of their interaction with thermal electrons and neutrals.
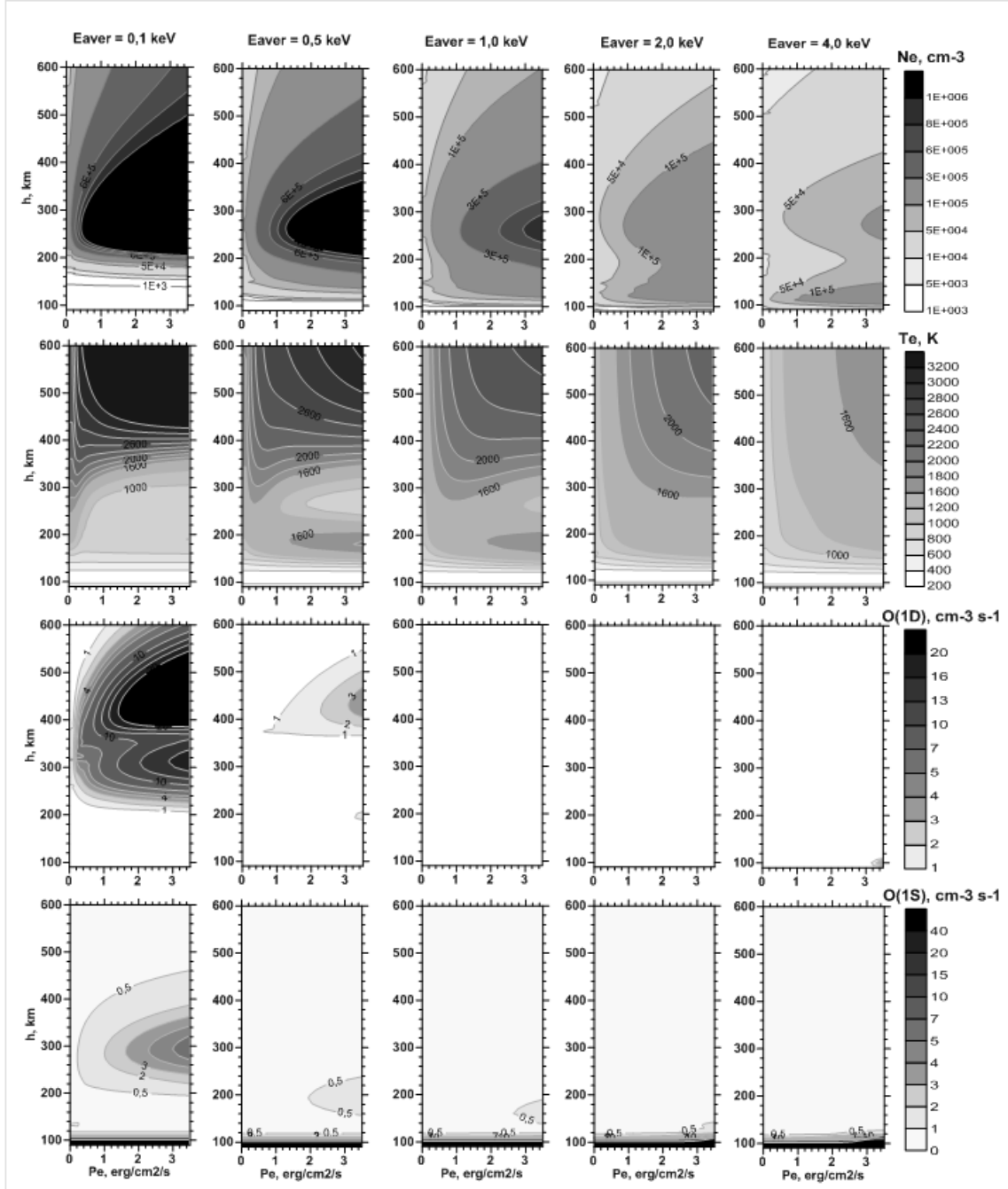

Figure 3. Estimated distributions of electron density n_e, electron temperature T_e, volume emission in the red O(^{1}D) and green O(^{1}S) lines at different average energies of precipitating electrons

Below ~200 km there are virtually no effects from precipitation of "soft" electrons. Above and below the height of the maximum, the electron density drops sharply to $n_e \leq 10^5$ cm^{-3}.

The electron temperature during very "soft" precipitation events (E_{aver}=0.1 keV) increases abruptly to $T_e \geq 3000$ K at $h \geq 300$ km, where precipitating electrons lose their energy most effectively. As the mean beam energy rises, STE penetrate into lower heights with a high content of neutral atoms and molecules, which in turn leads to the rapid formation of secondary electrons. This produces an additional heating source in the lower ionosphere ($h \leq 200$ km), which causes T_e to increase at these heights.

For "hard" precipitation events ($E_{aver} \geq 1$ keV), the STE penetration depth into the atmosphere increases. In this case, the area of effective energy losses is shifted down to $h \leq 150$ km, thus providing secondary electrons with the predominant role in the interaction of STE with thermal electrons and neutrals. As a result, vertical $n_e(h)$ profiles acquire two maxima – the upper one near 250 km and the lower one between 120–140 km. The vertical electron temperature gradient above 150 km decreases as both E_{aver} and P_e increase. In general, the level of electron density and temperature in the ionosphere produced by "hard" precipitation is approximately two times smaller than that produced by "soft" precipitation.

Two bottom rows of panels in Figure 3 illustrate variations in vertical profiles of volume emission in the atomic oxygen red and green lines, which are associated with variations in the integrated flux of precipitating electrons and their average energy. The figure shows that the "hard" precipitation ($E_{aver} \geq 1$ keV) does not generate atomic oxygen airglow. In the presence of "soft" precipitation, the vertical profile of volume emission in the red line exhibits two maxima.
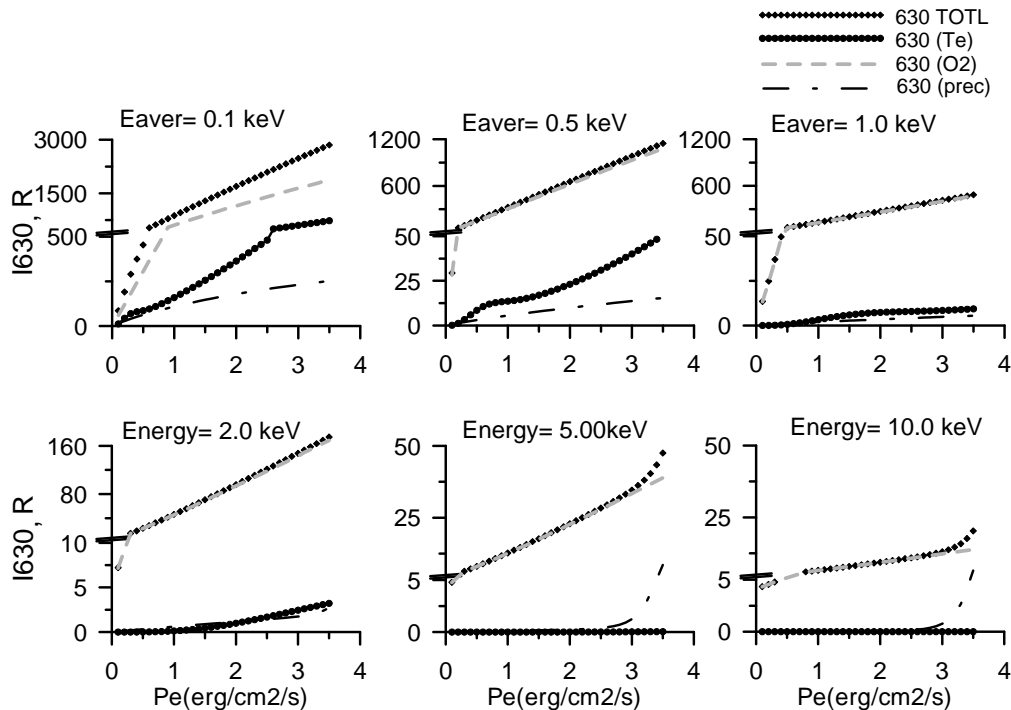

Figure 4. Estimated integrated emission intensity of the atomic oxygen red line O(^1D) as a function of beam energy at different average energies of precipitating electrons

The upper maximum with the most intense emission is located above 400 km and is due to two factors – the ^1D excitation by heated thermal electrons and the impact ionization by precipitating electrons, whereas the lower maximum arises from dissociative recombination of O_2^+ ions. The vertical profile of volume emission in the green line also has two maxima for "soft" precipitation. The lower maximum existing regardless of the presence of precipitation events is caused by triple collisions; and the upper one arises from the O_2^+ dissociative recombination. With increasing average beam energy ("hard" precipitation) the upper maximum disappears.

Figure 4 shows the estimated integrated intensity of the atomic oxygen red line as a function of the integral beam energy P_e and with different average energies of precipitating electrons E_{aver}. The calculations are made taking into account the following three processes of excitation of the atomic oxygen level ^1D:

- collision with thermal electrons, formula (9); in Figure 4, to it corresponds the 630 nm line (T_e);
- dissociative recombination of molecular ions O_2^+, formula (10); in Figure 4, to it corresponds the 630 nm line (O_2);
- collision of oxygen atoms with superthermal electrons, formula (11); in Figure 4, to it corresponds the 630 nm line (prec).

Figure 4 shows that the main contribution to the integrated intensity of the atomic oxygen red line emission is made by the reaction of dissociative recombination of the molecular ions O_2^+. It may also be noted that for the events displayed in Figure 2, the increase in the red line emission intensity to ≥ 200 R can be caused by the influence of precipitating electron fluxes with average energies $E_{aver} \leq 1$ keV.

Thus, precipitation events generate airglow in red and green lines not through the direct excitation of the metastable ^1D and ^1S levels by electron impact, but indirectly, through an increase in rates of ion production and thermal electron heating which, in turn, cause an increase in the rate of dissociative recombination and excitation of ^1D in collisions with thermal electrons.

REFERENCES

Banks P.M., Chappell C.R., Nagy A.F. A new model for the interaction of auroral electrons with the atmosphere: Spectral degradation, backscatter, optical emission, and ionization. *J. Geophys. Res.* 1974, vol. 79, iss. 10, pp. 1459–1470.

Hasegawa A. Particle acceleration by MHD surface wave and formation of aurorae. *J. Geophys. Res.* 1976, vol. 81, iss. 28, pp. 5083–5090.

Goertz C.K. Kinetic Alfv'en waves on auroral field lines. *Planet. Space Sci.* 1984, vol. 32, pp. 1387–1392.

Krinberg I.A. *Kinetika elektronov v ionosfere i atmosfere Zemli* [Kinetics of electrons in Earth's ionosphere and plasmasphere]. Moscow, Nauka Publ., 1978, 215 p. (In Russian).

Krinberg I.A., Tashchilin A.V. *Ionosfera i plazmosfera* [Ionosphere and plasmasphere]. Moscow, Nauka Publ., 1984. 188 p. (In Russian).

Leonovich A.S., Mazur V.A. Resonance excitation of standing Alfven waves in an axisymmetric magnetosphere (monochromatic oscillations). *Planet. Space Sci.* 1989, vol. 37, pp. 1095–1108.

Leonovich L.A., Mikhalev A.V., Leonovich V.A. Manifestation of geomagnetic disturbances in mid-latitude

upper atmosphere airglow. *Solnechno-zemnaya fizika* [Solar-Terrestrial Phys.]. 2012, vol. 20, pp. 109–115. (In Russian).

Leonovich L.A., Tashchilin A.V., Leonovich V.A. Response of 557.7 and 630 nm atomic oxygen emissions to sharp variations in solar wind parameters. *Atmos. Ocean. Optics.* 2015, vol. 28, no. 4, pp. 376–380.

de Meneses F.C., Muralikrishna P., Clemesha B.R. Height profiles of OI 630 nm and OI 557.7 nm airglow intensities measured via rocket-borne photometers and estimated using electron density data: comparison. *Geofisica Internacional.* 2008, vol. 47, no. 3, pp. 161–166.

Fox J.L., Sung K.Y. Solar activity variations of the Venus thermosphere/ionosphere. *J. Geophys. Res.: Space Phys.* 2001, vol. 106, iss. A10, pp. 21305–21335.

Hierl P.M., Dotan I., Seeley J.V., et al. Rate constants for the reactions of O^+ with N_2 and O_2 as a function of temperature (300–1800 K). *J. Chem. Phys.* 1997, vol. 106, no. 9, pp. 3540–3544.

Mantas G.P. Large 6300-Å airglow intensity enhancements observed in Ionosphere Heating Experiments are excited by thermal electrons. *J. Geophys. Res.: Space Phys.* 1994, vol. 99, iss. A5, pp. 8993–9002.

Picone J.M., Hedin A.E., Drob D.P., Aikin A.C. NRLMSISE-00 empirical model of the atmosphere: Statistical comparisons and scientific issues. *J. Geophys. Res.* 2002, vol. 107, iss. A12, pp. SIA 15-1–SIA 15-16.

Rees M.H. *Physics and Chemistry of the Upper Atmosphere*. Cambridge University Press., 1989, 289 p.

Richards P.G. Reexamination of ionospheric photochemistry. *J. Geophys. Res.* 2011, vol. 116, iss. A8, A08307.

Schunk R., Nagy A. *Ionospheres* . Cambridge University Press., 2009, 628 p.